Anisotropic lattice changes in femtosecond laser inscribed Nd^{3+}:MgO:LiNbO$_3$ optical waveguides

A. Ródenas,[1] L. M. Maestro,[1] M. O. Ramírez,[1] G. A. Torchia,[2] L. Roso,[3] F. Chen,[4] and D. Jaque[1,a]

[1]*Departamento de Física de Materiales, GIEL, Facultad de Ciencias, Universidad Autónoma de Madrid, Campus de Cantoblanco, Madrid 28049, Spain*
[2]*Centro de Investigaciones Ópticas, CONICET-CIC, 1900 La Plata, Argentina*
[3]*Grupo de Óptica, Facultad de Ciencias Físicas, Universidad de Salamanca, 37008 Salamanca, Spain*
[4]*School of Physics, Shandong University, 250100 Jinan, People's Republic of China*

We report on the fabrication and microspectroscopy imaging of femtosecond laser written double-filament based Nd^{3+}:MgO:LiNbO$_3$ optical waveguides. The waveguiding high refractive-index regions are identified by blueshifts of the Nd^{3+} ion fluorescence lines with no deterioration in the fluorescence efficiency, whereas filamentary low-index regions are identified by both a Nd^{3+} line redshift and a fluorescence efficiency reduction. The lattice structural micromodifications at the origin of both waveguide formation and Nd^{3+} fluorescence changes have been investigated by means of confocal micro-Raman experiments. We have found that the direct laser written filaments are mainly constituted by a large density of defects, together with a marked axial compression perpendicular to the filaments (along the optical *c*-axis). Conversely, the high-index waveguiding regions are characterized by a pronounced anisotropic dilatation of the LiNbO$_3$ lattice *xy*-planes. © *2009 American Institute of Physics*. [DOI: 10.1063/1.3168432]

I. INTRODUCTION

Lithium niobate (LiNbO$_3$, hereafter LN) is one of the most attractive dielectric media in modern optoelectronics due to its excellent nonlinear and electro-optic coefficients which make it an outstanding system for efficient optical conversion with the additional possibility of electrical driven index modulation.[1] LN crystals can also be doped with magnesium oxide and neodymium ions (Nd^{3+}:MgO:LiNbO$_3$, hereafter Nd:MgO:LN), in such a way that the crystal becomes a photorefractive-damage-resistant laser gain medium.[2–5] In addition to this, the fabrication of waveguides in Nd:MgO:LN crystals, and the subsequent light confinement achieved, would increase the nonlinear frequency conversion efficiencies and would simultaneously lead to a reduction in the laser threshold. Up to now, several methods have been applied to the fabrication of waveguides in LN crystals including thermal in-diffusion of Nd^{3+}, Ti^{3+} and ZnO$_2$,[6–8] ion implantation,[9,10] UV irradiation,[11] proton exchange,[12] or direct laser writing (DLW) with ultrafast laser pulses.[13] Among the different methods, the DLW technique presents clear advantages such as reduced fabrication times, direct three-dimensional (3D) design possibilities, and the absence of sample manipulation, or any multistep fabrication process. DLW of channel waveguides in LN crystals has been already demonstrated under different experimental conditions and configurations.[13–17] In particular, highly symmetric waveguides preserving the original nonlinear coefficients of the LN matrix and featuring strong resistance have been reported by the so-called *double line* design. This waveguide fabrication approach is based on the direct inscription of two parallel low refraction-index channels which are surrounded by strained high-index LN, in such a way that the region between them leads to a highly symmetric and homogeneous waveguide channel.[18,19] Despite previous works, the particular patterns of strain which arise from this kind of processing of the LN matrix have not yet been measured, and little is still known about the exact refraction-index change mechanisms.

The application of the double line approach to the fabrication of laser waveguides in Nd^{3+} doped LN crystals has been not hitherto been explored. Rare-earth ion doping is of special interest not only for elucidating the extent to which the applied fabrication method deteriorates the fluorescence properties of neodymium laser ions, and hence to determine the potential application of the obtained waveguides, but also because of the possibility of using the fluorescent ions as optical probes through the analysis of their luminescence properties, which can be used in order to gain further knowledge over the microstructural changes induced in the crystal lattice, and over the refractive-index change mechanisms. In the case of LN, understanding the laser induced refractive-index changes is far from being simple, as such a change can be caused by different processes such as local changes in the molar polarizability and in the molar density, by local modifications of the spontaneous polarization, by changes in the local composition, or by creation of local lattice damage in the LN network.[20–22]

In this work we have fabricated highly symmetric double line waveguides in a neodymium doped MgO:LiNbO$_3$ crystal. Scanning confocal microphotoluminescence (μ-PL) experiments have been carried out in order to elucidate how the Nd^{3+} fluorescence is affected by the ultrafast inscription procedure and how these changes are related to the index change

---

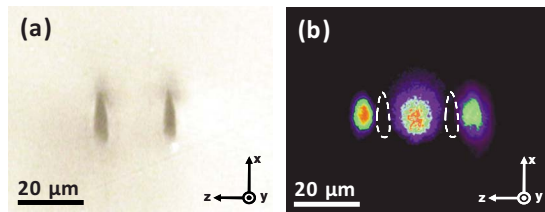a)Electronic mail: daniel.jaque@uam.es.

FIG. 1. (Color online) (a) Optical transmission micrograph of the double-filament structure fabricated by femtosecond laser writing in a $Nd:LiNbO_3$ crystal. (b) Near-field intensity distribution of the waveguides' modes at 632.8 nm.

mechanism. The spatial localization and extension of the different induced microstructural modifications obtained from the fluorescence images have been compared with the spatial extension and location of the waveguides' modes. To understand and relate these results, confocal micro-Raman (μ-Raman) experiments have also been performed, which allow getting deeper detail over the ultrafast laser inscription process and refractive-index change mechanisms, and explain the observed Nd^{3+} fluorescence changes.

II. EXPERIMENTAL

The buried channel waveguides under study in this work were fabricated in x-cut $Nd:MgO:LiNbO_3$ crystals with a Nd^{3+} and MgO concentrations of 0.3 at. % and 5 mol %, respectively. Waveguides were fabricated by using an amplified Ti:sapphire laser system providing 120 fs pulses at 796 nm and 1 kHz of repetition rate. The laser beam was focused with a $10\times$ microscope objective (numerical aperture, NA $=0.3$) and the translation of the sample was performed by an XYZ motorized stage with a spatial resolution of 0.2 μm. Under these conditions the waveguides are then fabricated in the nonthermal regime.[14] The linear focus of the objective was located 500 μm below the sample surface. The two damage tracks were written separated by 20 μm and by translating the sample with a speed of 50 μm/s in directions parallel to the crystallographic y-axis. The polarization of the writing femtosecond laser beam was perpendicular to the translation direction, i.e., parallel to the optical c-axis. The peak laser fluence was set to 35 J/cm^2 corresponding to a pulse energy of 1 μJ, which led to the creation of ≈ 20 μm length filaments. Figure 1(a) shows a microscope optical transmission image of the double line waveguide's end-face. The ability of the resulting structure as an optical waveguide was investigated by end-coupling experiments using a He–Ne laser (632.8 nm).

Due to the high fluorescence quantum yield of Nd^{3+} ions, confocal μ-PL allows for a fast and direct imaging of the intensity, linewidth, and energy spatial distributions of the emission peaks of Nd^{3+} laser ions at the waveguide's cross section. For this purpose, an Olympus BX-41 confocal microscope was used in combination with an XY motorized stage with a spatial resolution of ~ 100 nm. The 10 mW continuous wave 488 nm radiation from an argon laser was focused 10 μm deep from the sample surface by using a $50\times$ objective with numerical aperture NA=0.75. In this configuration the 488 nm laser radiation excites the Nd^{3+} ions from their ground state ($^4I_{9/2}$) up to the $^2G_{3/2}$ excited
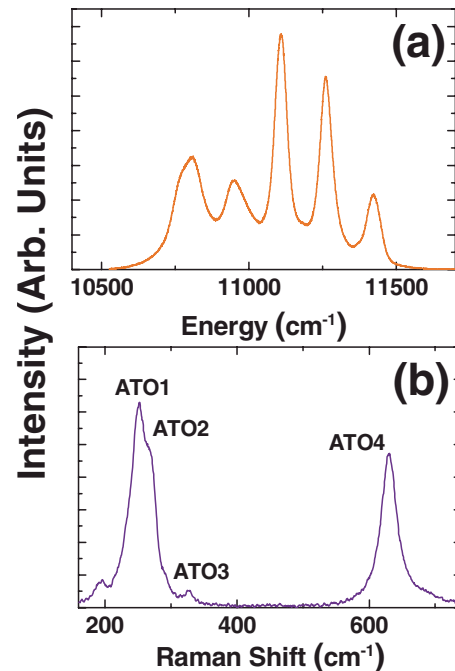

FIG. 2. (Color online) Typical a μ-luminescence (a) and μ-Raman (b) spectra obtained from the $Nd:LiNbO_3$ system in our experimental conditions. The different Raman modes contributing to our μ-Raman spectrum are properly labeled in (b).

state. Then the subsequent $^4F_{3/2} \rightarrow {}^4I_{9/2}$ emission band from Nd^{3+} ions is back-collected by the same microscope objective and analyzed on a high resolution spectrometer [see Fig. 2(a)]. The same microscope setup was used for μ-Raman backscattering measurements, with an additional set of notch filters and polarizers. Figure 2(b) shows a typical μ-Raman spectrum corresponding to the $y(zz)y$ configuration. In this figure the main four Raman modes contributing to the spectrum have been labeled according to prior works.[23–25] 3D spectral maps [line intensity, full width at half maximum (FWHM), and energy] were obtained by fitting the collected spectra and plotting the obtained values with the aid of LAB-SPEC© and WSMP© softwares.[26]

III. RESULTS AND DISCUSSION

A. Waveguide optical characterization

Figure 1(b) shows a composed image of the near-field intensity distributions of the three waveguide modes observed. Waveguiding occurs at the laterals of each filament, so that in this configuration it led to two types of waveguides: between filaments (quasisymmetric central mode) and at their external laterals (asymmetric lateral modes). These three waveguiding areas could only be excited individually by translating the sample, so that evanescent coupling was not observed. In the three cases waveguiding was observed for both TM and TE polarizations. Figure 1(b) reflects the fact that the refractive index has been increased at both sides of the filaments. The absence of evanescent coupling suggests an important refractive-index decrease at filaments. This is, in fact, in agreement with the refractive-index map previously assumed for double-filament LN waveguides.[27]
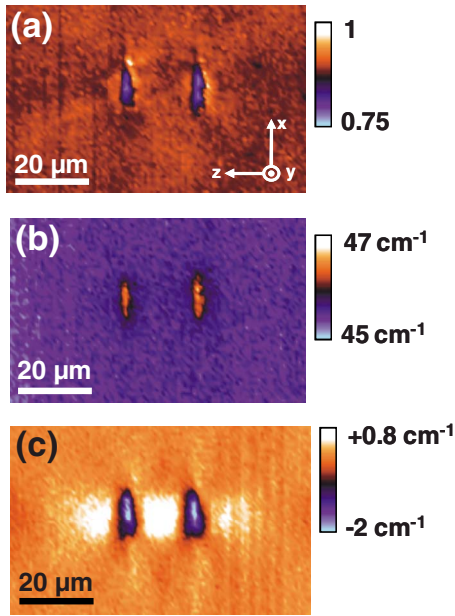
FIG. 3. (Color online) Spatial distribution of the intensity (a), linewidth (b), and position (c) of the main Nd^{3+} luminescence peak within the $^4F_{3/2}$ $\rightarrow$ $^4I_{9/2}$ band located at around 11 100 cm^{-1}.

FIG. 4. (Color online) Spectral shift induced in the main Nd^{3+} luminescence peak within the $^4F_{3/2} \rightarrow ^4I_{9/2}$ band (located at around 11100 cm^{-1}) as obtained along the horizontal scan schematically shown by a solid arrow on the top image. The position of filaments is indicated by the vertical shaded lines.

B. Microfluorescence

The fluorescence images of the double-filament based waveguide are shown in Fig. 3. Figure 3(a) shows the spatial distribution of the integrated intensity of the Nd^{3+} fluorescence main emission peak at around 11 100 cm^{-1}. From this image it is clear that the fluorescence intensity is only inhomogeneous at the filaments, where a significant reduction has been experimentally observed. This local fluorescence reduction is accompanied by a relevant linewidth increase, as shown in Fig. 3(b). Both intensity reductions and line broadening indicate that filaments are constituted by a partially damaged volume characterized by a higher defect density and by local disordering of the Nd:MgO:LN network.[28] These observations are in agreement with the conclusions recently extracted from the microspectroscopy analysis of similar waveguides fabricated in Nd^{3+}:YAG ceramics.[29] From Fig. 3(a) it is clear that the fluorescence efficiency of Nd^{3+} ions is, however, very well preserved at the waveguide volume (i.e., between filaments and at their laterals). The absence of any Nd^{3+} fluorescence quenching surrounding the femtosecond laser focal regions is also a characteristic feature of the ultrafast DLW method, and it also reflects the fact that the laser properties of Nd^{3+} ions at waveguiding region are not deteriorated, and thus that the fabricated waveguides are reasonable good candidates for low-threshold integrated laser sources. This fact constitutes a significant advantage over other waveguide fabrication methods previously applied to the Nd^{3+}:LN system, such as proton exchange, which have been found to cause significant deterioration of the Nd^{3+} fluorescence properties.[30]

While the intensity and linewidth of the emission peaks of Nd^{3+} ions are only observed to change inside the femtosecond laser focal volumes, the spectral position of the Nd^{3+} emission lines can react to changes not associated with dam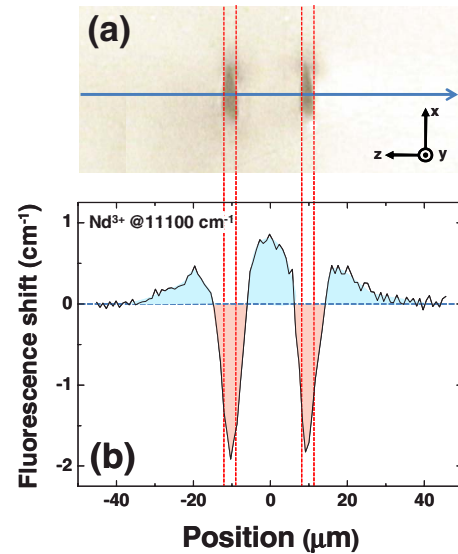age, but to extremely small alterations of the crystal field symmetry and strength around the Nd^{3+} ions. In this case [see Fig. 3(c)] the damaged filaments are characterized by a strongly marked redshift of the Nd^{3+} emission lines, whereas a blueshift is observed at both sides of them, matching with the waveguiding high refractive-index regions. For easier visualization of the effect, Fig. 4 shows a cross section of the fluorescence energy shift map. According to previous works a red-/blueshift of the Nd^{3+} emission lines in LN can be unequivocally related to a local increment/reduction in the crystalline field affecting the Nd^{3+} ion sites.[28,31] As a consequence, data of Figs. 3(c) and 4 indicate that, in a first order approximation, the crystal field affecting Nd^{3+} ions has been increased at filaments (where refractive index has been reduced) and decreased at the waveguides' location (where refractive index has been increased). Thus, it is reasonable to link, in this particular case, the mechanism at the origin of crystalline field reduction to the mechanism causing a local refractive-index increment at waveguides' location. However, no conclusions about the origin of waveguiding can be obtained so far from these observations, as the spectral shifts in the Nd^{3+} fluorescence can be attributed to a large variety of processes, such as anisotropic compressions or dilatations of the LN network, slight changes in the Nd^{3+} ion site location within the LN unit cell, ionic rearrangement of the LN network constituents, or to changes in the local LN composition.[28,31–34] In order to elucidate in which way the LN network has been perturbed in these modified areas, and hence to elucidate the waveguide formation origin, we have performed μ-Raman measurements (described in Sec. III C). μ-Raman spectral analysis is a powerful tool for the detection of local lattice modifications in chemical composition, unit cell volume, ionic displacements, local disorder, or extended defects.

C. μ-Raman

The $y(zz)y$ polarized μ-Raman spectrum of Nd:MgO:LN crystals is constituted by four transverse optical (TO) Raman modes, as indicated in Fig. 2(b). According to previous works these four modes correspond to vibrations along the z-axis of Nb ions against the O sublattice leaving Li relatively static (ATO_1 mode), antiphase vibrations along the z-axis of Li and Nb ions with respect to the O ions (ATO_2 mode), to rigid rotations of the whole O ion octahedron along the c-axis (ATO_3 mode), and to stretching vibrations of the O octahedron along the xy-plane (ATO_4 mode).[23,24,35,36] A general response of all these Raman modes to the presence of extended defects within the LN network is a decrease in intensity.[37] In addition, the presence of structural disorder in the LN lattice will broaden all the observed Raman modes.[38] Consequently, a detailed analysis of the μ-Raman properties could provide precise information about what kind of lattice rearrangements and/or damage is present in the DLW LN waveguides.

The variation in the Raman properties in the waveguides and filaments has been studied by imaging the waveguide cross section. From the obtained maps a linear cross section crossing both the waveguides and filaments at their medium point has been extracted, which are shown in Fig. 5. Figures 5(b) and 5(c) depict the integrated Raman intensity and the FWHM of the ATO_4 Raman mode, respectively. Very similar profiles were obtained when the other Raman modes were analyzed. It is clear from these profiles that a sharp reduction in the integrated Raman intensity is produced at the filaments, this being accompanied by a relevant spectral broadening of Raman modes. As previously mentioned, these two facts indicate that a large density of extended defects has been induced at filaments, in addition to a local disordering of the Nd:MgO:LN network. This means that a slight degree of crystal amorphization has been induced at filament locations. This conclusion is, indeed, in good agreement with the simultaneous reduction and broadening of the Nd^{3+} fluorescence lines [see Figs. 3(a) and 3(b)]. The presence of a large density of defects at the femtosecond laser focal volume has been also observed in other ultrafast laser inscribed waveguides fabricated in undoped LN and $LiTaO_3$ crystals.[38,39] In this sense, it is clear that filaments are constituted by a partially damaged Nd:MgO:LN volume which, according to previous studies, is characterized by a reduced refractive index.[21]

In Fig. 6 we have included the profiles obtained for the spatial distribution of the energy shifts of the Raman modes. It is clear that the energy shift of the four Raman modes depicts relevant modifications of dissimilar nature at the filaments and at their surroundings, where waveguides have been created. The observed changes in terms of the Raman modes energy shifts can be summarized as follows.

(i)   *At filaments.* All the Raman modes shift to higher vibration energies with respect to their surroundings. A net blueshift of the Raman modes with respect to bulk nonirradiated zones is mainly observed for the Raman modes involving only ionic displacements or rotations along the c-axis (i.e., the ATO_2, and ATO_3 Raman
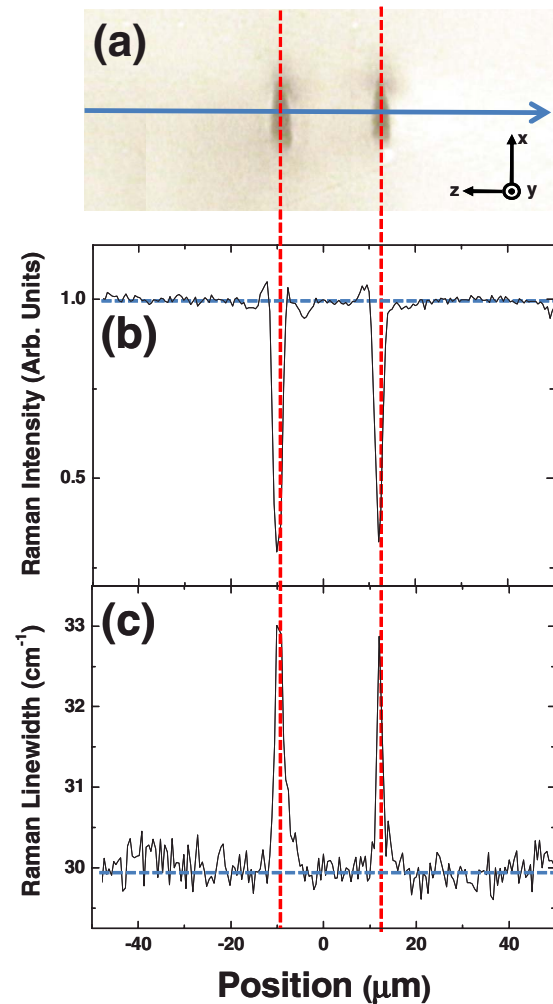

FIG. 5. (Color online) (a) Schematic drawing of the scan direction along which Raman measurements have been done. Spatial dependence of the integrated Raman intensity (b) and of the ATO_4 linewidth (c). Similar results, not shown for the sake of brevity, have been obtained when the spatial distribution of the linewidth of the other Raman modes has been analyzed.

modes). The strong blueshift of the ATO_2 (~ 2.15 cm^{-1}) can be interpreted in a first order approximation as an axial compression of the LN unit cell along the optical c-axis, which in this case coincides with the perpendicular plane to filaments. This compression well explains the observed redshift of Nd^{3+} ions at the filaments (see Figs. 3 and 4).

(ii) *At waveguide location.* The ATO_1, ATO_3, and ATO_4 Raman modes are significantly redshifted, whereas the ATO_2 Raman mode shows a remnant blueshift as a collateral effect to the nonisotropic compression at the filaments. According to these spatial distributions it is reasonable to conclude that at waveguides' location a nonisotropic distortion of the Nd:MgO:LN network has been produced. This anisotropic distortion is characterized by (a) an enlargement in the distances between Nb ions and the O sublattice [denoted by the redshift in the ATO_1 Raman mode (~ -0.69 cm^{-1})], and in the distances defining the oxygen octahedron lying in the xy-plane [denoted by the redshift in the ATO_4 Raman mode (~ -0.67 cm^{-1})], and (b) by a
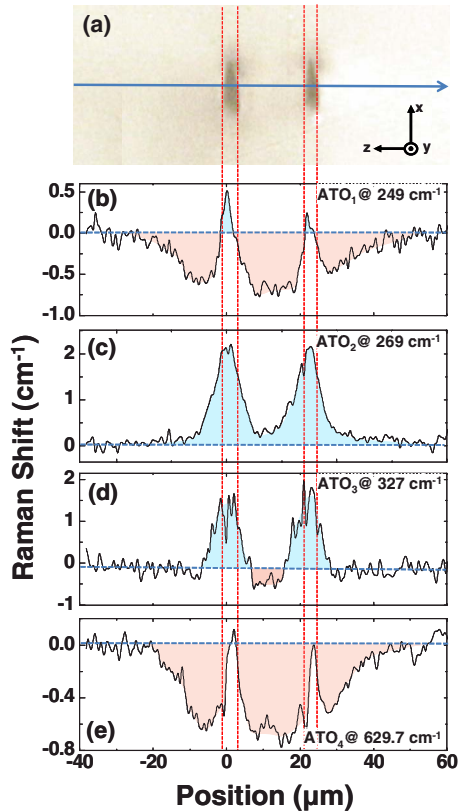
FIG. 6. (Color online) (a) Schematic drawing of the scan direction through waveguide and filaments. (b) Spatial distribution of the energy shift of the four Raman modes under study in this work. The vertical dashed lines indicate the location of filaments.

slight reduction in the distance between Li and Nb ions along the z-axis [denoted by the blueshift of the ATO_2 Raman mode (~ 0.30 cm^{-1})]. The fact that this anisotropic distortion leads to a strong Nd^{3+} blueshift [see Fig. 3(c)], in contrast to the redshift observed at compressed filaments, let us conclude that the main strain pattern responsible for the observed increased refractive-index regions is that of a LN lattice dilatation along the laser writing vertical direction, which in this case coincides with the x-axis of the LN network. This effect is, in fact, consistent with an overall increment in the distance between Nd^{3+} ions and their closest neighbors that explains the observed blueshifts at the waveguides location.

Thus, the analysis of the μ-Raman image profiles denotes that in the double line waveguides under study in this work, a dominant anisotropic compression/dilatation of the Nd:MgO:LN network has been produced at filament/waveguiding areas characterized by a refractive-index decrease/increment. This scenario is quite different to that previously assumed for double line waveguides fabricated in LN crystals.[27] In that case it was assumed that a volume increase was taking place at filaments (i.e. at the laser focal volume), and this density decrease was assumed to produce the observed refractive-index reduction at filaments. The focal volume expansion was then stated to induce a local compression of the LN network at the sides of the filaments,

causing an elasto-optic refractive-index increment which could explain waveguiding for TM polarization.[27] In our case, the mechanism leading to waveguide formation for both polarizations (TM and TE) appears to be different. At filaments, an anisotropic axial compression has been observed, whereas at waveguide position an anisotropic lattice dilatation is observed. Although it is not possible to unequivocally conclude from our data the general mechanism of the local increment in the refractive-index, we state that the refractive-index increment has been likely caused by a local variation in the spontaneous polarization and electronic polarizability due to the nonisotropic distortion of the LN network. This mechanism has been also assumed to be at the origin of the refractive-index modification in ion implanted LN waveguides,[40] and it was also assumed to be responsible for the formation of waveguides in LN crystals fabricated by ultrafast inscription in the thermal regime with high-repetition rate infrared lasers, where similar redshifts of about -0.7 cm^{-1} in the Raman ATO_1 and ATO_4 modes were also observed at waveguide location.[36] In addition, a similar assumption of slight ionic rearrangements in the LN lattice was also previously accepted as the most plausible mechanism for waveguide formation after ion implantation.[41] Finally, it is worth noting that this proposed waveguide formation mechanism entails only a very small Raman modification at waveguide position, and therefore suggests that the Nd:MgO:LN lattice well preserves its original nonlinear and photorefractive properties.[42]

IV. CONCLUSIONS

In summary, we report on the fabrication and microspectroscopy characterization of Nd^{3+}:MgO:LiNbO$_3$ optically active waveguides by the ultrafast "double-filament" DLW technique in the nonthermal regime. We have demonstrated that the ultrafast inscription method does not modify the fluorescence efficiency of neodymium ions at waveguides' volume, making the fabricated structures promising candidates for the future development of multifunctional integrated laser sources. The combination of microluminescence and μ-Raman analysis has been used to elucidate in detail the microstructural anisotropic modifications induced in the lithium niobate network as a consequence of the ultrashort pulse laser processing. We have found that the DLW filaments constitute anisotropically compressed volumes in which a slight lattice amorphization induces the strong refractive-index decrease. While this anisotropic compression at filaments is observed to be linked to a significant redshift of the Nd^{3+} ion emission line, the laser induced lattice defects and disorder are associated with the Nd^{3+} ions fluorescence efficiency reduction. On the other hand, the situation at the laterals of filaments, where the refractive-index increment and waveguide have been created, is found to be significantly different; in these areas the nonisotropic distortion of the lithium niobate network mainly consists on a dilatation along the xy lattice planes in complete absence of any induced lattice disorder or defects. This different strain pattern is also observed to be accompanied by a marked blueshift of the Nd^{3+} ion emission. Based on these observa-

tions we have stated that the mechanism at the origin of the refractive-index increment is likely to be a change in the electronic polarizability and in the spontaneous polarization of the lithium niobate network. Further investigations need to be done in order to unveil the exact process underlying the observed refractive-index increments.

ACKNOWLEDGMENTS

[1] *Properties of Lithium Niobate*, edited by K. K. Wong (IEE, London, UK, 2002).

[2] T. R. Volk, V. J. Pryalkin, and M. N. Rubinina, Opt. Lett. **15**, 996 (1990).

[3] D. Jaque, J. A. Sanz, and J. García Solé, Appl. Phys. Lett. **85**, 19 (2004).

[4] D. Jaque, J. Capmany, J. A. Sanz García, A. Brenier, G. Boulon, and J. García Sole, Opt. Mater. (Amsterdam, Neth.) **13**, 147 (1999).

[5] E. Lallier, J. P. Pocholle, M. Papuchon, C. Grezes-Besset, E. Pelletier, M. De Micheli, M. J. Li, Q. He, and D. B. Ostrowsky, Electron. Lett. **25**, 1491 (1989).

[6] M. Hempstead, J. S. Wilkinson, and L. Reekie, IEEE Photonics Technol. Lett. **4**, 852 (1992).

[7] R. Regener and W. Sohler, Appl. Phys. B **36**, 143 (1985).

[8] E. Cantelar, J. A. Sanz García, G. Lifante, F. Cussó, and P. L. Pernas, Appl. Phys. Lett. **86**, 161119 (2005).

[9] F. Chen, X. L. Wang, and K. M. Wang, Opt. Mater. (Amsterdam, Neth.) **29**, 1523 (2007).

[10] L. Wang, K. M. Wang, F. Chen, X. L. Wang, L. L. Wang, H. Liu, and Q. M. Lu, Opt. Express **15**, 16880 (2007).

[11] S. Mailis, C. Riziotis, I. T. Wellington, P. G. R. Smith, C. B. E. Gawith, and R. W. Eason, Opt. Lett. **28**, 1433 (2003).

[12] A. di Lallo, A. Cino, C. Conti, and G. Assanto, K. El Hadi, A. C. Cino, P. Aschieri, and D. B. Ostrowsky, Opt. Express **8**, 232 (2001).

[13] L. Gui, B. Xu, and T. C. Chong, IEEE Photonics Technol. Lett. **16**, 1337 (2004).

[14] A. H. Nejadmalayeri and P. R. Herman, Opt. Express **15**, 10842 (2007).

[15] R. R. Thomson, S. Campbell, I. J. Blewett, A. K. Kar, and D. T. Reid, Appl. Phys. Lett. **88**, 111109 (2006).

[16] A. H. Nejadmalayeri and P. R. Herman, Opt. Lett. **31**, 2987 (2006).

[17] R. Osellame, M. Lobino, N. Chiodo, M. Marangoni, G. Cerullo, R. Ramponi, H. T. Bookey, R. R.Thomson, N. D. Psaila, and A. K. Kar, Appl. Phys. Lett. **90**, 241107 (2007).

[18] J. Thomas, M. Heinrich, J. Burghoff, S. Nolte, A. Ancona, and A. Tünnermann, Appl. Phys. Lett. **91**, 151108 (2007).

[19] J. Burghoff, C. Grebing, S. Nolte, and A. Tuennermann, Appl. Phys. Lett. **89**, 081108 (2006).

[20] V. V. Atuchin, Nucl. Instrum. Methods Phys. Res. B **168**, 498 (2000).

[21] P. D. Townsend, P.J. Chandler, and L. Zhang, *Optical Effects of Ion Implantation* (Cambridge University Press, Cambridge, 1994).

[22] C. Kittel, *Introduction to Solid State Physics*, 8th ed. (Wiley, New York, 2005).

[23] Y. Zhang, L. Guilbert, P. Bourson, K. Polgar, and M.D. Fontana, J. Phys.: Condens. Matter **18**, 957 (2006).

[24] V. Caciuc, A.V. Postnikov, and G. Borstel, Phys. Rev. B **61**, 8806 (2000).

[25] F. Abdi, M. Aillerie, P. Bourson, M. D. Fontana, and K. Polgar, J. Appl. Phys. **84**, 2251 (1998).

[26] I. Horcas, R. Fernandez, J. M. Gomez-Rodriguez, J. Colchero, J. Gomez-Herrero, and A. M. Baro, Rev. Sci. Instrum. **78**, 013705 (2007).

[27] J. Burghoff, S. Nolte, and A. Tünnermann, Appl. Phys. A **89**, 127 (2007).

[28] B. Henderson and G. F. Imbusch, *Optical Spectroscopy of Inorganic Solids* (Oxford Science, New York, 1989); A. Ródenas, J. A. Sanz García, D. Jaque, G. A. Torchia, C. Mendez, I. Arias, L. Roso, and F. Agulló-Rueda, J. Appl. Phys. **100**, 033521 (2006).

[29] A. Ródenas, G. A. Torchia, G. Lifante, E. Cantelar, J. Lamela, F. Jaque, L. Roso, and D. Jaque, Appl. Phys. B: Lasers Opt. **95**, 85 (2009).

[30] E. M. Rodríguez, D. Jaque, E. Cantelar, F. Cussó, G. Lifante, A. C. Busacca, A. C. Cino, and S. Riva Sanseverino, Opt. Express **15**, 8805 (2007).

[31] U. R. Rodríguez Mendoza, A. Ródenas, D. Jaque, I. R. Martín, F. Lahoz, and V. Lavín, High Press. Res. **26**, 341 (2006).

[32] H. Loro, M. Voda, F. Jaque, J. Garcia Sole, and J. E. Muñoz Santiuste, J. Appl. Phys. **77**, 5929 (1995).

[33] A. Lorenzo, H. Loro, J. E. Muñoz Santiuste, M. C. Terrile, G. Boulon, L. E. Bausa, and J. Garcia Sole, Opt. Mater. (Amsterdam, Neth.) **8**, 55 (1997).

[34] J. Garcia Sole, L. E. Bausa, D. Jaque, E. Montoya, H. Murrieta, and F. Jaque Spectrochim. Acta, Part A **54**, 1571 (1998).

[35] I. Savova, I. Savatinova, and E. Liarokapis, Opt. Mater. (Amsterdam, Neth.) **16**, 353 (2001).

[36] A. Jayaraman and A. A. Ballman, J. Appl. Phys. **60**, 1208 (1986).

[37] S. M. Kostritskii and P. Moretti, Phys. Status Solidi C **1**(11), 3126 (2004).

[38] A. Ródenas, A. H. Nejadmalayeri, D. Jaque, and P. Herman, Opt. Express **16**, 13979 (2008).

[39] B. McMillen, K. Chen, and D.Jaque, Appl. Phys. Lett. **94**, 081106 (2009).

[40] Y. Jiang, K.-M. Wang, X.-L. Wang, F. Cheng, C.-L. Jia, L. Wang, and Y. Jiao, Phys. Rev. B **75**, 195101 (2007).

[41] D. Jaque, F. Chen, and Y. Tan, Appl. Phys. Lett. **92**, 161908 (2008).

[42] W. D. Johnston, Jr., Phys. Rev. B **1**, 3494 (1970).